Higher-Radix Chrestenson Gates for Photonic Quantum Computation

Kaitlin N. Smith, Tim P. LaFave Jr., Duncan L. MacFarlane, and Mitchell A. Thornton
Quantum Informatics Research Group
Southern Methodist University
Dallas, TX, USA
{knsmith, tlafave, dmacfarlane, mitch}@smu.edu

Abstract

A recently developed four-port coupler used in optical signal processing applications is shown to be equivalent to a Chrestenson operator, or gate, in radix-4 quantum information processing (QIP) applications. The radix-4 qudit is implemented as a location-encoded photon incident on one of the four ports of the coupler. The quantum informatics transfer matrix is derived for the device based upon the conservation of energy equations when the coupler is employed in a classical sense in an optical communications environment. The resulting transfer matrix is the radix-4 Chrestenson transform, and this operator is capable of placing a radix-4 qudit in a state of maximal superposition. This result indicates that a new practical device is available for use in the implementation of radix-4 QIP applications or in the construction of a radix-4 quantum computer.

1 Introduction

In the field of quantum computing, theory has been well developed over the last half-century. There is still room for the discovery of new operators and algorithms, but current work is enough to show the potential that quantum methods have for solving some of the most difficult scientific problems. Unfortunately, the physical implementations for QIP have not advanced as rapidly as the theory. Since a standard platform has not been chosen for the quantum computer (QC), efforts have been divided among many competing technologies with quantum optics being one of the more promising physical realizations. This work hopes to contribute a new,

higher-radix component to the already well-established photonic quantum computing library.

The four-port coupler is an optical component shown theoretically to act as a quantum gate that can place a radix-4 photon-encoded qudit into a state of equal superposition. The gate realized optically is known as the radix-4 Chrestenson gate, and its transfer function is derived from the generalized radix-r Chrestenson transformation. Many QIP techniques require quantum superposition, so this operator is significant to the field of quantum computing due to the need to evolve information into a state of superposition for quantum algorithm execution. A description of the four-port coupler as well as a demonstration of its capabilities as a quantum optics operator will be shown mathematically in this work.

This paper proceeds as follows. A brief summary of important QIP concepts, details of the Chrestenson gate, with emphasis on the radix-4 implementation, and information about quantum optics are provided in Section 2. The four-port coupler, the component of interest, is described in Section 3. The physical realization of the four-port coupler with optical elements, including its fabrication and characterization, is included in Section 4. The demonstration of the four-port coupler as a radix-4 Chrestenson gate is presented in Section 5. Finally, a summary with conclusions can be found in Section 6. This paper is an extension of the work originally published in reference [1].

2 Quantum theory background

2.1 The qubit vs. qudit

The quantum bit, or qubit, is the standard unit of information for radix-2, or base-2, quantum computing. The qubit models information as a linear combination of two orthonormal basis states such as the states $|0\rangle$ and $|1\rangle$. $|0\rangle$ and $|1\rangle$ are Dirac notation representations where $|0\rangle = \begin{bmatrix} 1 & 0 \end{bmatrix}^{\mathrm{T}}$ and $|1\rangle = \begin{bmatrix} 0 & 1 \end{bmatrix}^{\mathrm{T}}$, respectively. The qubit differs from the classical bit by its ability to be in a state of superposition, or a state of linear combination, of all basis states. Superposition allows QIP algorithms to be very powerful since it allows for parallelism during computation so that multiple combinations of information can be evaluated at once. In other words, a single QC taking advantage of superposition can complete some tasks in a time frame that would require multiple classical computers working simultaneously. There are theoretically an infinite number of states for a qubit while in a state of superposition

$$|\Psi\rangle = x\,|0\rangle + y\,|1\rangle = \begin{bmatrix} x & y \end{bmatrix}^{\mathrm{T}} \tag{1}$$

where x and y are complex values, $c \in \mathbb{C}$, such that $c = a + ib$ where i is an imaginary number, $i^2 = -1$. For the qubit $|\Psi\rangle$, the probability that $|\Psi\rangle = |0\rangle$ is equal to $x^*x = |x|^2$ and the probability that $|\Psi\rangle = |1\rangle$ is equal to $y^*y = |y|^2$ where the symbol * indicates a complex conjugate. The total probability of occupying either one basis state or the other must total to 100%, so the inner product, or dot product, of $|\Psi\rangle$ with itself must equal 1. In other words, $x^*x + y^*y = 1$. Once a qubit is measured, it collapses into a basis state as defined by the eigenvectors of the measurement operator [2]. The measurement operation causes a qubit's state of superposition to be lost.

Qubits are the current standard for encoding data in QIP, but it is possible to have a quantum system of higher order. Increasing the radix during computation allows for higher density data to be transmitted because more information is stored in each fundamental unit of information, or digit, of the system [3]. A quantum unit of dimension, or radix, $r > 2$ is referred to as a qudit. In this paper, the radix-4 qudit using four orthonormal basis states is of interest. The set of basis states used for the radix-4 qudit includes the vectors $|0\rangle = \begin{bmatrix}1 & 0 & 0 & 0\end{bmatrix}^{\mathrm{T}}$, $|1\rangle = \begin{bmatrix}0 & 1 & 0 & 0\end{bmatrix}^{\mathrm{T}}$, $|2\rangle = \begin{bmatrix}0 & 0 & 1 & 0\end{bmatrix}^{\mathrm{T}}$, and $|3\rangle = \begin{bmatrix}0 & 0 & 0 & 1\end{bmatrix}^{\mathrm{T}}$. Just like the radix-2 qubit, the radix-4 qudit is not limited to having the value of only one of its four possible basis states. The qudit is capable of existing in a linear combination, or a state of superposition, of all four basis states, as demonstrated by

$$|\Phi\rangle = v\,|0\rangle + x\,|1\rangle + y\,|2\rangle + z\,|3\rangle = \begin{bmatrix}v & x & y & z\end{bmatrix}^{\mathrm{T}} \tag{2}$$

where v, x, y, and z are complex values. These coefficients can be multiplied by their respective complex conjugates in order to derive the probability that the radix-4 qudit is in a particular basis state. The basis state probabilities of $|\Phi\rangle$ must sum to 100%, so $v^*v + x^*x + y^*y + z^*z = 1$.

For a radix-4 quantum system to be physically realized, a methodology must exist for encoding four distinct qudit basis states. In reference [4], Rabi oscillations are utilized to create radix-r quantum systems. Orbital angular momentum (OAM) states of light could also be used to encode the qudit [5]. In this paper, a radix-4 quantum state will be created using the location of light as the information carrier. This technique builds on the concept of the quantum photonic dual-rail representation of the qubit in order to physically realize the radix-4 qudit with a quad-rail implementation.

2.2 Quantum operations

According to the most popular quantum computing paradigm proposed in reference [6], a quantum state must be prepared by a QC in a known basis. Afterwards, meaningful information is generated by evolving to the quantum state through quantum operations. After all computations are complete, the quantum state must be able to be measured to produce an output. If a quantum algorithm is modeled as a circuit, quantum operations can be viewed as quantum logic gates. Each of these gates is represented by a unique, unitary transfer function matrix, $\mathbf{U}$, that is characterized by the following properties:

- $\mathbf{U}^\dagger\mathbf{U} = \mathbf{U}\mathbf{U}^\dagger = \mathbf{I}_r$
- $\mathbf{U}^{-1} = \mathbf{U}^\dagger$
- $\text{Rank}(\mathbf{U}) = r$
- $|\mathbf{U}| = 1$

When considering radix-r quantum operations, or gates, the transfer function matrices will always be square matrices each of a dimension that is a power of r. Therefore, radix-4 qudit operations will have a dimension that is a power of four, 4^k, where the power, k, indicates the amount of qudits transformed by the quantum operation.

2.3 The Chrestenson gate

The power of QIP lies in the ability for a quantum state to be in superposition, and achieving states of maximal superposition is of especially high importance because it is typically one of the first steps required in quantum algorithms. When the probability amplitudes are all nonzero and the square of their magnitudes are equivalent, the qubit or qudit is said to be maximally superimposed, or is in maximal superposition, with respect to some basis set. Practically, this means that the qubit or qudit is equally likely to be measured at the value of any of the possible basis vectors.

In radix-2 quantum computation, the Hadamard gate

$$\mathbf{H} = \frac{1}{\sqrt{2}} \begin{bmatrix} 1 & 1 \\ 1 & -1 \end{bmatrix} \tag{3}$$

is an important operator used to put a qubit in a maximally superimposed state. When a qubit originally in a basis state passes through the Hadamard gate, the

transformed quantum information has equal probability of being observed, or measured, as either $|0\rangle$ or $|1\rangle$. Quantum operators exist for many different computation bases, such as radix-3 and above, that achieve equal, and therefore maximal, superposition among the corresponding basis states. These operators are derived using the discrete Fourier transform on Abelian groups. General theory of Fourier transforms on Abelian groups is outlined in the literature [7, 8]. The multiple-valued generalization of the radix-2 quantum Hadamard gate and its transfer matrix is composed of discretized versions of the orthogonal Chrestenson basis function set [8]. This QIP gate is generally referred to as the Chrestenson gate [9]. Examples of useful applications of the Chrestenson transform in QIP can be found in reference [10].

The Chrestenson operator, as the generalized version of the Hadamard operator, has a shape that depends on the radix of computation. The resulting radix-r Chrestenson transformation matrix for a single qudit has a size of $r \times r$, and the basis vectors that span the matrix are composed of r different values. Since the Chrestenson transformation matrix is normalized with a scalar factor, $\frac{1}{\sqrt{r}}$, and the matrix is orthogonal, both the column and row vectors of the operator form an orthonormal set. Each of the components within a Chrestenson transform matrix is one of the r^{th} roots of unity raised to an integral power [8, 9]. The r^{th} roots of unity can be visualized as r points that are evenly-spaced on the unit circle in the complex plane. The roots of unity are indicated as w_k where $k = 0, 1, ..., (r-1)$, and the point (1,0), denoted as w_0, is always included in this set. Each root satisfies $(w_k)^r$ as roots of one. The closed-form representation of the r^{th} roots of unity for a radix-r Chrestenson transformation is

$$w_k = e^{i\frac{2\pi}{r}\times k}. \tag{4}$$

Fig. 1 contains the plots for the r^{th} roots of unity for $r = 2, 3, 4$, and 5.

The structure of the Chrestenson transform matrix is in the form of a Vandermonde matrix where each row vector consists of a r^{th} root of unity, w_k, raised to an integral power j. Each element of the matrix is some form of w_k^j where j is the column index and k is the row index. In this indexing scheme, $j = 0$ is assigned to the leftmost column vector and $j = (r-1)$ is assigned to the rightmost column vector. Similarly, $k = 0$ is assigned to the topmost row vector and $k = (r-1)$ is assigned to the bottommost row vector. It can be observed that the Hadamard matrix results from the Chrestenson transform matrix with $r = 2$, confirming that the Chrestenson transform is a generalization of the Hadamard transform for higher-dimensional quantum systems. The generalized radix-r Chrestenson transform matrix, $\mathbf{C_r}$, is

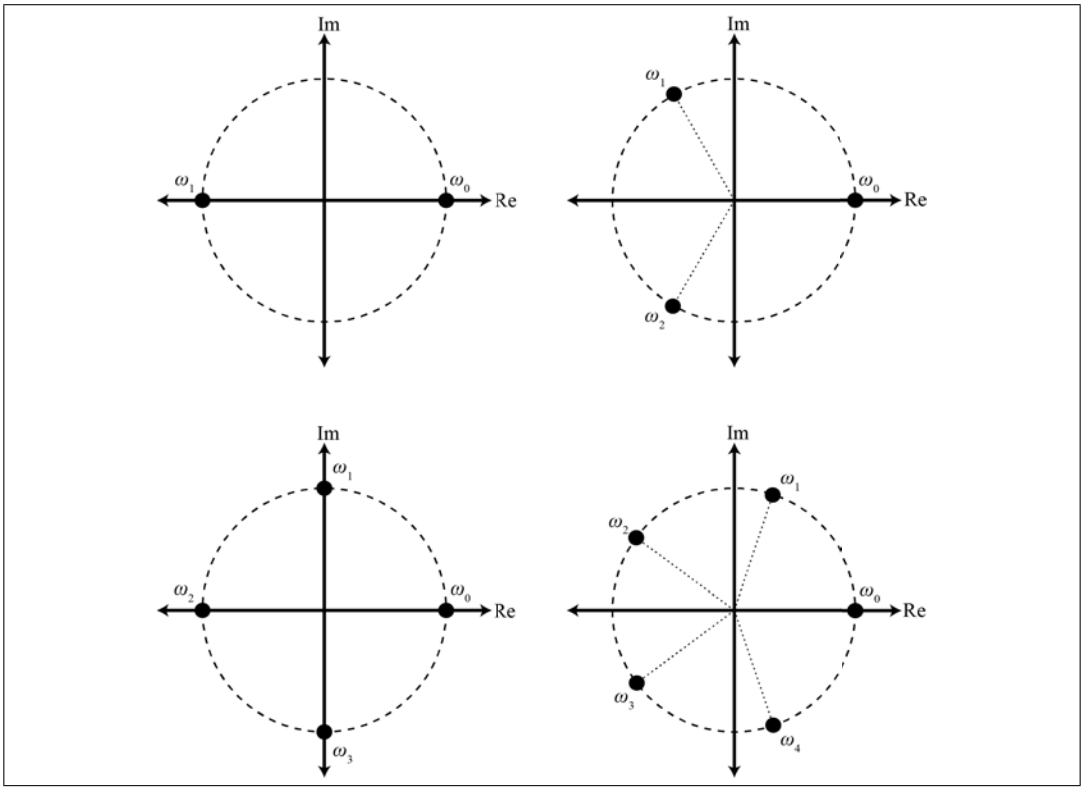

Figure 1: Roots of unity in the complex plane for $r = 2, 3, 4$, and 5.

represented with a matrix in the form of

$$\mathbf{C}_r = \frac{1}{\sqrt{r}} \begin{bmatrix} w_0^0 & w_0^1 & \dots & w_0^{(r-1)} \\ w_1^0 & w_1^1 & \dots & w_1^{(r-1)} \\ \vdots & \vdots & \ddots & \vdots \\ w_{(r-1)}^0 & w_{(r-1)}^1 & \dots & w_{(r-1)}^{(r-1)} \end{bmatrix}. \tag{5}$$

Using the fourth roots of unity, $w_0 = \exp[(i2\pi/4) * 0] = 1$, $w_1 = \exp[(i2\pi/4) * 1] = i$, $w_2 = \exp[(i2\pi/4) * 2] = -1$, and $w_3 = \exp[(i2\pi/4) * 3] = -i$, in Eq. 5, the radix-4

Chrestenson gate transfer matrix becomes

$$\mathbf{C_4} = \frac{1}{\sqrt{4}} \begin{bmatrix} 1 & 1 & 1 & 1 \\ 1 & i & -1 & -i \\ 1 & -1 & 1 & -1 \\ 1 & -i & -1 & i \end{bmatrix}. \tag{6}$$

The radix-4 Chrestenson gate ($\mathbf{C_4}$), allows a radix-4 qudit originally in a basis to evolve into a quantum state of equal superposition. The following example shows how the radix-4 qudit $|a\rangle = |0\rangle$ evolves to $|b\rangle = \frac{1}{2}|0\rangle + \frac{1}{2}|1\rangle + \frac{1}{2}|2\rangle + \frac{1}{2}|3\rangle$, taking the value of the first column of the radix-4 Chrestenson matrix, after passing through the $\mathbf{C_4}$ transform

$$\mathbf{C_4}\,|a\rangle = |b\rangle\,,$$

$$\mathbf{C_4}\,|0\rangle = \frac{1}{\sqrt{4}} \begin{bmatrix} 1 & 1 & 1 & 1 \\ 1 & i & -1 & -i \\ 1 & -1 & 1 & -1 \\ 1 & -i & -1 & i \end{bmatrix} \begin{bmatrix} 1 \\ 0 \\ 0 \\ 0 \end{bmatrix} = \frac{1}{2} \begin{bmatrix} 1 \\ 1 \\ 1 \\ 1 \end{bmatrix},$$

$$\mathbf{C_4}\,|0\rangle = \frac{1}{2}[|0\rangle + |1\rangle + |2\rangle + |3\rangle].$$

If $|a\rangle = |3\rangle$, the radix-4 qudit would evolve to $|b\rangle = \frac{1}{2}|0\rangle - \frac{1}{2}i\,|1\rangle - \frac{1}{2}|2\rangle + \frac{1}{2}i\,|3\rangle$, taking the value of the last column of the $\mathbf{C_4}$ transformation matrix.

$$\mathbf{C_4}\,|3\rangle = \frac{1}{\sqrt{4}} \begin{bmatrix} 1 & 1 & 1 & 1 \\ 1 & i & -1 & -i \\ 1 & -1 & 1 & -1 \\ 1 & -i & -1 & i \end{bmatrix} \begin{bmatrix} 0 \\ 0 \\ 0 \\ 1 \end{bmatrix} = \frac{1}{2} \begin{bmatrix} 1 \\ -i \\ -1 \\ i \end{bmatrix},$$

$$\mathbf{C_4}\,|3\rangle = \frac{1}{2}[|0\rangle - i\,|1\rangle - |2\rangle + i\,|3\rangle].$$

The schematic symbol of the $\mathbf{C_4}$ gate is pictured in Fig. 2. This symbol can be used in radix-4 quantum circuit diagrams.

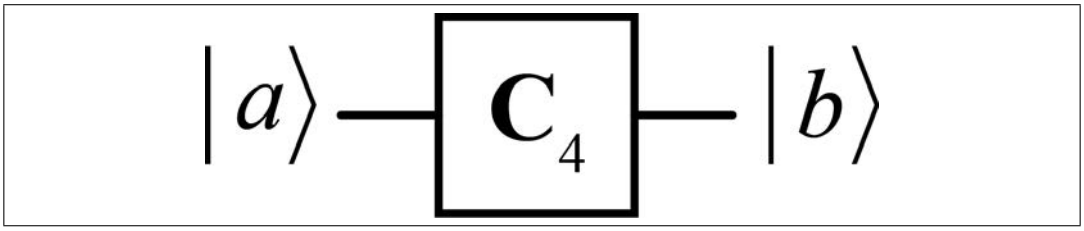

Figure 2: Symbol of the radix-4 Chrestenson gate, $\mathbf{C_4}$.

2.4 Quantum optics

Optical quantum implementations are among the more successful physical realizations of quantum states. In these systems, orthogonal basis states can be encoded into photon OAM states, polarization, or location, and the state can easily evolve by passing through linear optical elements. The photon resists coupling to other objects in its environment, allowing it to maintain its quantum state and not decohere for long periods of time [11]. Additionally, the ability to maintain coherence enables the photon to travel great distances at room temperature, making it a good candidate for long-haul quantum information transmission.

Although photons offer the benefit of state stability in QIP applications, their failure to interact with their surroundings prevents them from coupling with each other. Photon-to-photon interaction is difficult, limiting the development of reliable controlled multi-qubit, or multi-qudit in higher radix systems, gate implementations. Without operations such as the radix-2 controlled-NOT (CNOT) gate or the controlled-phase gate, a functional QC cannot exist.

It was once thought that photonic quantum computation was unachievable without nonlinear optical elements, but the presentation of the KLM protocol in reference [12] improved the outlook for quantum optics. In that work, a methodology for implementing photonic multi-qubit operations using linear optics was introduced. These multi-qubit photonic gates, however, are unfortunately limited by probabilistic operation. Currently, the two-qubit CNOT operation can only work 1/4 of the time when implemented with linear optical elements in the best case scenario [13].

The subject of this paper is a photonic radix-4 Chrestenson gate. Since this quantum operator is formed from linear optical elements and transforms a single qudit at a time, the gate is theoretically deterministic in nature.

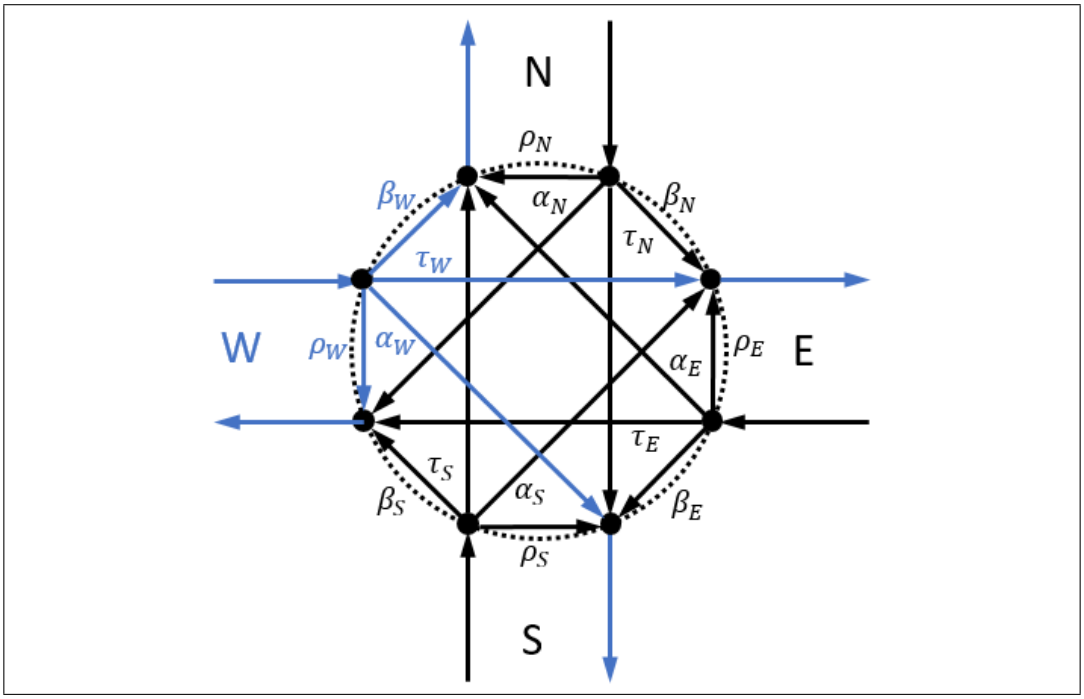

Figure 3: Signal flow for four-port coupler with input at W.

3 The four-port coupler

The four-port coupler is an optical component introduced and described in reference [14]. This device is composed of four inputs and four outputs where the input and output are referred to by their orientation on the component of either W, N, E, or S. When a single beam is sent into one of the coupler inputs, the component routes a fraction of the original signal to each of the four outputs. This beam division is caused by the transmission and reflection of signals within the coupler. Each fraction of the input beam seen at an output corresponds to one of the following components of the original signal: a reflected component ρ, a transmitted component τ, a right-directed component α, and a left-directed component β. An illustration of signal flow of the four-port coupler can be seen in Fig. 3. This image is recreated from a figure included in reference [14].

Fig. 3 demonstrates in blue a signal entering the four-port coupler from the W port and exiting the component from the W, N, E, and S ports. The output signals are generated by ρ_W, β_W, τ_W, and α_W, respectively. Whenever a single input enters the component, all four coupling coefficients are generated to produce four outputs.

The coupling coefficients produced with a particular port input can be derived with the coupling coefficient matrix,

$$\begin{bmatrix} \rho_W & \alpha_N & \tau_E & \beta_S \\ \beta_W & \rho_N & \alpha_E & \tau_S \\ \tau_W & \beta_N & \rho_E & \alpha_S \\ \alpha_W & \tau_N & \beta_E & \rho_S \end{bmatrix}. \tag{7}$$

To produce the outputs, an input vector taking the form of $[WNES]^{\mathrm{T}}$ is multiplied by the matrix in Eq. 7 to create a column vector of coupling coefficients. The produced output column vector also takes the form of $[WNES]^{\mathrm{T}}$. The composition of the output vector in terms of coupling coefficients indicates what portion of the input signal contributes to an output from a port.

The four-port coupler does not consume nor dissipate any of the energy that is input into the component. Therefore, to conserve energy, all of the energy entering the element must be equal to the energy leaving the element. This concept leads to the creation of equations that act as conditions that must hold true for energy conservation. The 10 energy conservation equations of Eqs. 8-17, first derived in reference [14], use the coupling coefficients found in the matrix of Eq. 7. These equations are:

$$\rho_W^* \rho_W + \beta_W^* \beta_W + \tau_W^* \tau_W + \alpha_W^* \alpha_W = 1, \tag{8}$$

$$\rho_N^* \rho_N + \beta_N^* \beta_N + \tau_N^* \tau_N + \alpha_N^* \alpha_N = 1, \tag{9}$$

$$\rho_E^* \rho_E + \beta_E^* \beta_E + \tau_E^* \tau_E + \alpha_E^* \alpha_E = 1, \tag{10}$$

$$\rho_S^* \rho_S + \beta_S^* \beta_S + \tau_S^* \tau_S + \alpha_S^* \alpha_S = 1, \tag{11}$$

$$\rho_W^* \tau_E + \beta_W^* \alpha_E + \tau_W^* \rho_E + \alpha_W^* \beta_E = 0, \tag{12}$$

$$\alpha_N^* \beta_S + \rho_N^* \tau_S + \beta_N^* \alpha_S + \tau_N^* \rho_S = 0, \tag{13}$$

$$\rho_W^* \alpha_N + \beta_W^* \rho_N + \tau_W^* \beta_N + \alpha_W^* \tau_N = 0, \tag{14}$$

$$\alpha_N^* \tau_E + \rho_N^* \alpha_E + \beta_N^* \rho_E + \tau_N^* \beta_E = 0, \tag{15}$$

$$\tau_E^* \beta_S + \alpha_E^* \tau_S + \rho_E^* \alpha_S + \beta_E^* \rho_S = 0, \tag{16}$$

and

$$\rho_W^* \beta_S + \beta_W^* \tau_S + \tau_W^* \alpha_S + \alpha_W^* \rho_S = 0. \tag{17}$$

The first four conditions seen in Eqs. 8-11 exist since the inner product of each produced field vector from a single input, W, N, E, and S, with itself must sum to 1 for energy conservation. The last six conditions seen in Eqs. 12-17 exist due to energy conservation that occurs whenever two inputs are present in the component. Since the coefficient vectors are orthogonal, the inner product between the two produced coupling coefficient vectors corresponding to inputs at two different ports must equal zero. There are only 6 constraints produced from sending two inputs to the four-port coupler because the input combinations are commutative (i.e. $AB = BA$). The cases of three inputs and four inputs into the four-port coupler do not create additional constraints, so they are omitted [14].

4 Physical realizations of the four-port coupler

A macroscopic realization of a four-port coupler is shown in Fig. 4. Whereas a popular implementation of a radix-2 Hadamard gate is an optical beam splitter, polarizing or not, the macroscopic four-port coupler is a unitary extension of a two-prism beam splitting cube. Here, the macroscopic four-port coupler is comprised of four right angle prisms, coated with an appropriate thin film, cemented together with care given to the precise mating of the four prism corners. This component has been used to demonstrate novel, four leg Michelson interferometers designed in reference [15].

Integrated photonic four-port couplers were previously demonstrated for applications in optical signal processing as part of a two-dimensional array of waveguides in a multi-quantum well (MQW) GaInAsP indium phosphide (InP) architecture [16, 17]. Fig. 5 shows an electron micrograph of a coupler fabricated at the intersection of two ridge waveguides.

The optical behavior of the four-port coupler depends on frustrated total internal reflection [18]. The evanescent field of light incident on the coupler is transfered across the width of the coupler that may be an air gap or a thin slice of dielectric. Provided the barrier width is small enough, a part of the exponentially decaying

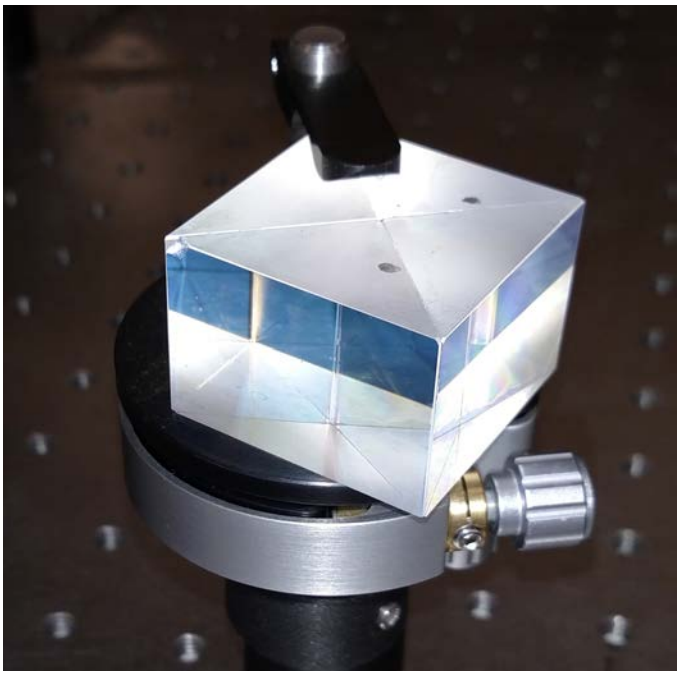

Figure 4: Macroscopic realization of a four-port coupler.

optical power of the incident light is transmitted across while the remaining optical power is reflected. Thus, a fraction of light incident on a four-port coupler may be transmitted to the ongoing waveguide, reflected to both perpendicular waveguides, or reflected back into the originating waveguide. The fractions of light in outbound waveguides are determined by the refractive indices of the waveguide and coupler materials in addition to the width of the coupler.

4.1 Fabrication

Fabrication of the coupler was performed in several steps using nanoelectronic processing techniques. First, coupler regions of 180 nm widths and 7 μm lengths were defined by patterning a thin metallic chromium mask layer atop the waveguides by focused ion beam (FIB) lithography. Precision alignment and orientation of the coupler to the waveguides during FIB processing was achieved with alignment markers fabricated beforehand with the waveguides using conventional microelectronic processing steps. High aspect ratio trenches were then etched using a hydrogen bromine (HBr) based [15] inductively coupled plasma (ICP) to a depth of 3.9 μm. This depth

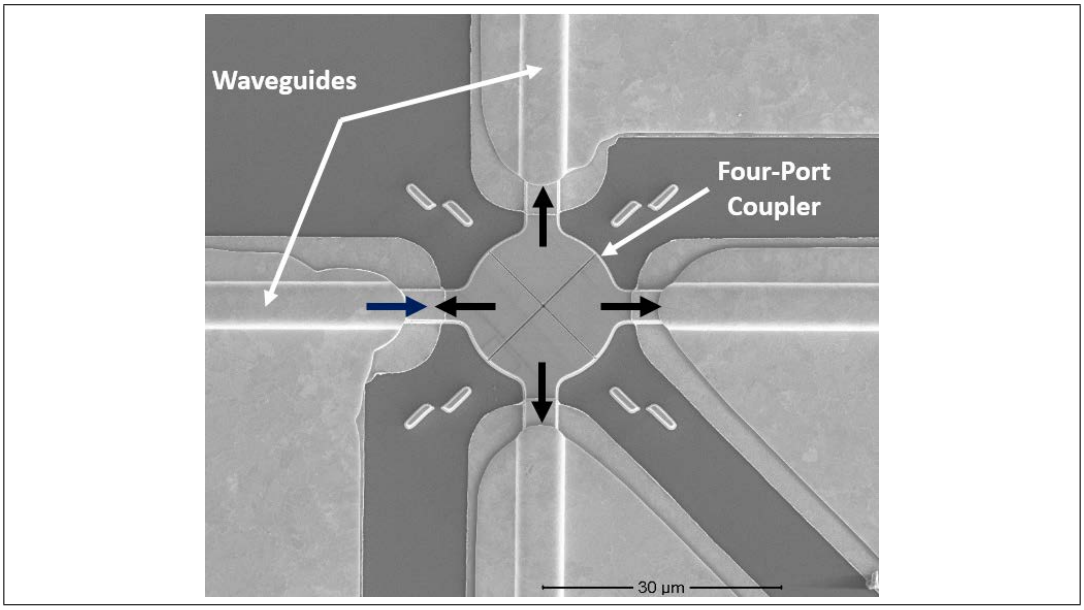

Figure 5: Cross sectional scanning electron microscope image of a four-port coupler in MQW-InP.

allows the coupler to fully cover optical modes confined to the quantum well region of the waveguides.

The optimal air gap width for 25% power on all output waveguides of about 90 nm was slightly smaller than the processing capability of the ICP dry etch tool for the required high-aspect ratio etch. Consequently, to meet this requirement for a wavelength of 1550 nm, alumina (Al_2O_3), with a refractive index of $n = 1.71$, was back-filled into the trench using atomic layer deposition (ALD). The resulting alumina-filled trench is shown in the composite cross-sectional transmission electron micrographs in Fig. 6.

4.2 Characterization

A 1550 nm laser was coupled into the waveguides using a tapered lens fiber at one input port. The near-field modes of light were coupled out of the device and into another tapered lens fiber for optical power measurement to characterize the coupling efficiency of the four-port coupler. The measured average power coefficients were $\alpha = 0.156$, $\beta = 0.140$, $\rho = 0.302$, and $\tau = 0.220$ for a measured total average coupling efficiency of 82% for the four-port coupler [16].

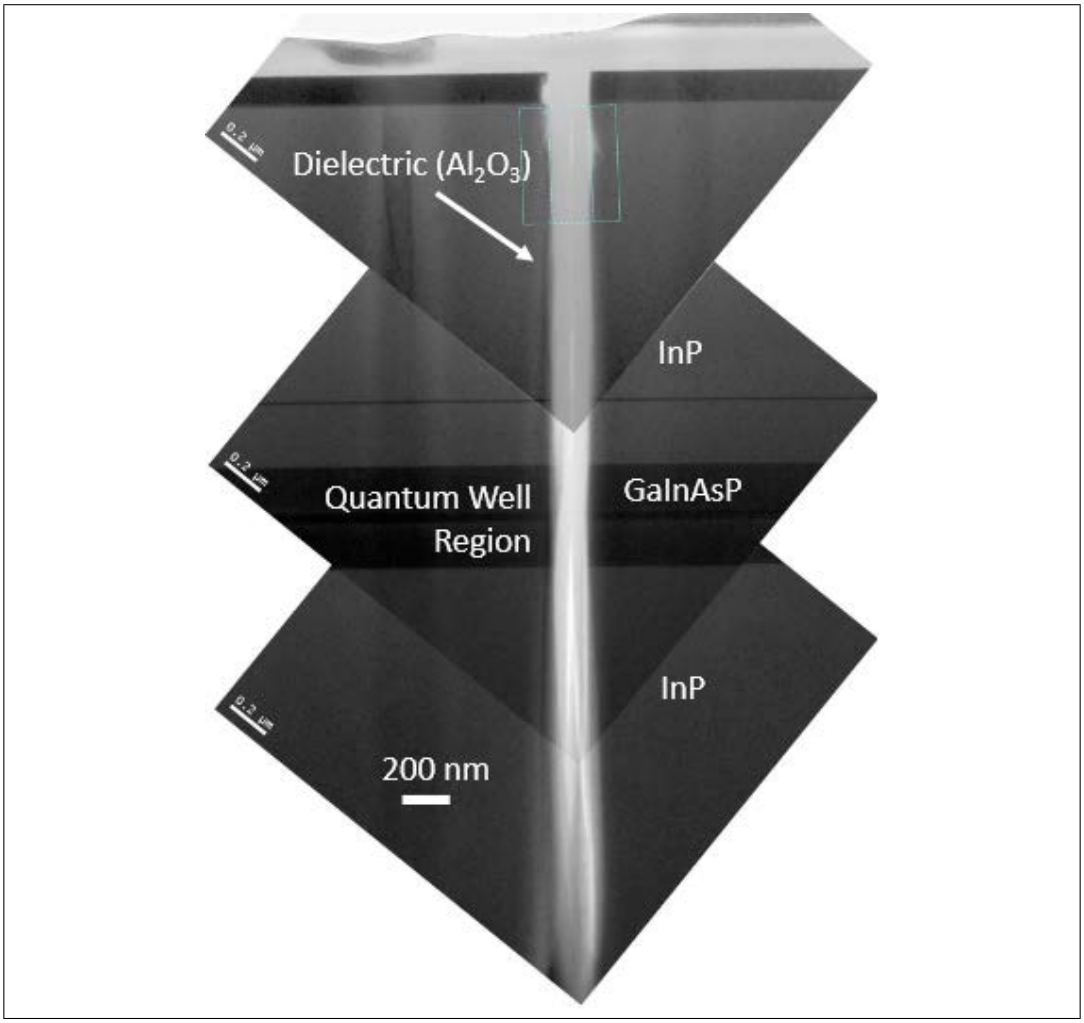

Figure 6: Cross sectional transmission electron micrograph of a four-port coupler backfilled with alumina using atomic layer deposition.

5 Implementing qudit quantum operations with the coupler

It is known that the Hadamard gate meant for use with a quantum qubit can be constructed from a beam splitter [11]. The radix-4 Chrestenson operation, an operation that acts on a quantum encoding using four basis states, transforms a radix-4 qudit, and the four-port coupler is a physical realization of this gate. In the realization of

the radix-4 Chrestenson gate, the ports of the four-port coupler must be encoded in order to represent the four qudit basis states. In this paper, the following encoding has been chosen for the location-based scheme: port W is the $|0\rangle$ rail, port N is the $|1\rangle$ rail, port E is the $|2\rangle$ rail, and port S is the $|3\rangle$ rail.

The four-port coupler follows 10 energy conservation equations, Eqs. 8-17, that are algebraically nonlinear. If the radix-4 Chrestenson matrix values are substituted for the values of the coupling coefficients in Eq. 7, the energy conservation constraints are satisfied and the following matrix is generated:

$$\begin{bmatrix} \rho_W = \frac{1}{2} & \alpha_N = \frac{1}{2} & \tau_E = \frac{1}{2} & \beta_S = \frac{1}{2} \\ \beta_W = \frac{1}{2} & \rho_N = \frac{1}{2}i & \alpha_E = -\frac{1}{2} & \tau_S = -\frac{1}{2}i \\ \tau_W = \frac{1}{2} & \beta_N = -\frac{1}{2} & \rho_E = \frac{1}{2} & \alpha_S = -\frac{1}{2} \\ \alpha_W = \frac{1}{2} & \tau_N = -\frac{1}{2}i & \beta_E = -\frac{1}{2} & \rho_S = \frac{1}{2}i \end{bmatrix}.$$

When a single photon, representing a qudit, is applied to one of the inputs the four-port coupler, either W, N, E, or S, energy is conserved and the radix-4 Chrestenson transform is achieved. The photon leaves the gate with equal superposition of all basis states. In other words, the photon has a 1/4 probability of being located in any of the output ports W, N, E, or S representing the basis states $|0\rangle$, $|1\rangle$, $|2\rangle$, or $|3\rangle$, respectively:

$$\rho_W^*\rho_W + \beta_W^*\beta_W + \tau_W^*\tau_W + \alpha_W^*\alpha_W = 1,$$
$$\left(\frac{1}{2}\right)\left(\frac{1}{2}\right) + \left(\frac{1}{2}\right)\left(\frac{1}{2}\right) + \left(\frac{1}{2}\right)\left(\frac{1}{2}\right) + \left(\frac{1}{2}\right)\left(\frac{1}{2}\right) = 1,$$
$$\rho_N^*\rho_N + \beta_N^*\beta_N + \tau_N^*\tau_N + \alpha_N^*\alpha_N = 1,$$
$$\left(-\frac{1}{2}i\right)\left(\frac{1}{2}i\right) + \left(-\frac{1}{2}\right)\left(-\frac{1}{2}\right) + \left(\frac{1}{2}i\right)\left(-\frac{1}{2}i\right) + \left(\frac{1}{2}\right)\left(\frac{1}{2}\right) = 1,$$
$$\rho_E^*\rho_E + \beta_E^*\beta_E + \tau_E^*\tau_E + \alpha_E^*\alpha_E = 1,$$
$$\left(\frac{1}{2}\right)\left(\frac{1}{2}\right) + \left(-\frac{1}{2}\right)\left(-\frac{1}{2}\right) + \left(\frac{1}{2}\right)\left(\frac{1}{2}\right) + \left(-\frac{1}{2}\right)\left(-\frac{1}{2}\right) = 1,$$

$$\rho_S^*\rho_S + \beta_S^*\beta_S + \tau_S^*\tau_S + \alpha_S^*\alpha_S = 1,$$

$$\left(-\frac{1}{2}i\right)\left(\frac{1}{2}i\right)+\left(\frac{1}{2}\right)\left(\frac{1}{2}\right)+\left(\frac{1}{2}i\right)\left(-\frac{1}{2}i\right)+\left(-\frac{1}{2}\right)\left(-\frac{1}{2}\right)=1.$$

If two signals are input into the four-port coupler Chrestenson gate, the conservation of energy causes the inner product of the two produced vectors of coupling coefficients to be zero:

$$\rho_W^*\tau_E+\beta_W^*\alpha_E+\tau_W^*\rho_E+\alpha_W^*\beta_E=0,$$

$$\left(\frac{1}{2}\right)\left(\frac{1}{2}\right)+\left(\frac{1}{2}\right)\left(-\frac{1}{2}\right)+\left(\frac{1}{2}\right)\left(\frac{1}{2}\right)+\left(\frac{1}{2}\right)\left(-\frac{1}{2}\right)=0,$$

$$\alpha_N^*\beta_S+\rho_N^*\tau_S+\beta_N^*\alpha_S+\tau_N^*\rho_S=0,$$

$$\left(\frac{1}{2}\right)\left(\frac{1}{2}\right)+\left(-\frac{1}{2}i\right)\left(-\frac{1}{2}i\right)+\left(-\frac{1}{2}\right)\left(-\frac{1}{2}\right)+\left(\frac{1}{2}i\right)\left(\frac{1}{2}i\right)=0,$$

$$\rho_W^*\alpha_N+\beta_W^*\rho_N+\tau_W^*\beta_N+\alpha_W^*\tau_N=0,$$

$$\left(\frac{1}{2}\right)\left(\frac{1}{2}\right)+\left(\frac{1}{2}\right)\left(\frac{1}{2}i\right)+\left(\frac{1}{2}\right)\left(-\frac{1}{2}\right)+\left(\frac{1}{2}\right)\left(-\frac{1}{2}i\right),$$

$$\alpha_N^*\tau_E+\rho_N^*\alpha_E+\beta_N^*\rho_E+\tau_N^*\beta_E=0,$$

$$\left(\frac{1}{2}\right)\left(\frac{1}{2}\right)+\left(-\frac{1}{2}i\right)\left(-\frac{1}{2}\right)+\left(-\frac{1}{2}\right)\left(\frac{1}{2}\right)+\left(\frac{1}{2}i\right)\left(-\frac{1}{2}\right)=0,$$

$$\tau_E^*\beta_S+\alpha_E^*\tau_S+\rho_E^*\alpha_S+\beta_E^*\rho_S=0,$$

$$\left(\frac{1}{2}\right)\left(\frac{1}{2}\right)+\left(-\frac{1}{2}\right)\left(-\frac{1}{2}i\right)+\left(\frac{1}{2}\right)\left(-\frac{1}{2}\right)+\left(-\frac{1}{2}\right)\left(\frac{1}{2}i\right)=0,$$

$$\rho_W^*\beta_S+\beta_W^*\tau_S+\tau_W^*\alpha_S+\alpha_W^*\rho_S=0,$$

$$\left(\frac{1}{2}\right)\left(\frac{1}{2}\right)+\left(\frac{1}{2}\right)\left(-\frac{1}{2}i\right)+\left(\frac{1}{2}\right)\left(-\frac{1}{2}\right)+\left(\frac{1}{2}\right)\left(\frac{1}{2}i\right)=0.$$

Since these equations are satisfied with the elements of the derived radix-4 Chrestenson transform matrix, the four-port coupler proves to act as an effective radix-4 Chrestenson gate.

6 Conclusion

In this paper, an integrated photonic four-port coupler that has potential for integration in radix-4 qudit based quantum photonic circuits is discussed. By showing that the radix-4 Chrestenson transfer function satisfies the operational conditions imposed by the conservation of energy for the coupler, we demonstrate the component's ability to act as a radix-4 qudit Chrestenson gate in an optical quantum system. The Chrestenson gate puts a radix-r qudit into a state of equal superposition between all orthogonal basis states, so the discovery of a physical realization of such a gate is significant. Because a linear combination of radix-4 basis states can be achieved in quantum optics whenever the four-port coupler is used, QIP algorithms that utilize maximal qudit superposition can be realized with this element. The introduction of new quantum applications for the four-port coupler as a radix-4 Chrestenson gate will lead to additional gates and methods that make radix-4 quantum photonic systems more robust.

References

[1] K. N. Smith, T. P. LaFave, Jr., D. L. MacFarlane, and M. A. Thornton. A Radix-4 Chrestenson Gate for Optical Quantum Computation. *IEEE International Symposium on Multiple Valued Logic (ISMVL)*, pp. 260-265, 2018.

[2] M. A. Nielsen and I. L. Chuang. *Quantum Computation and Quantum Information.* Cambridge University Press, 2010.

[3] D. M. Miller and M. A. Thornton. *Multiple-Valued Logic Concepts and Representations.* Morgan & Claypool Publishers, 2008.

[4] K. Fujii. Quantum optical construction of generalized Pauli and Walsh-Hadamard matrices in three level systems. *arXiv preprint quant-ph/0309132*, 2003.

[5] J. C. García-Escartín and P. Chamorro-Posada. Quantum multiplexing with the orbital angular momentum of light. *Phys. Rev. A*, 78(6), 2008.

[6] D. Deutsch. Quantum theory, the Church-Turing principle and the universal quantum computer. *Proceedings of the Royal Society of London A: Mathematical, Physical and Engineering Sciences*, 400(1818): 97-117, 1985.

[7] N. Y. Vilenkin. Concerning a class of complete orthogonal systems. *Dokl. Akad. Nauk SSSR, Ser. Math*, 11, 1947.

[8] H. E. Chrestenson. A class of generalized Walsh functions. *Pacific Journal of Mathematics*, 5(1): 17-31, 1955.

[9] Z. Zilic and K. Radecka. Scaling and better approximating quantum Fourier transform by higher radices. *IEEE Trans. on Computers*, 56(2): 202-207, 2007.

[10] Z. Zilic and K. Radecka. The Role of Super-fast Transforms in Speeding up Quantum Computations. *IEEE International Symposium on Multiple Valued Logic (ISMVL)*, pp. 129-135, 2002.

[11] P. Kok, W. J. Munro, K. Nemoto, T. C. Ralph, J. P. Dowling, and G. J. Milburn. Linear optical quantum computing with photonic qubits. *Rev. of Mod. Phys.*, 79(1): 135-174, 2007.

[12] E. Knill, R. Laflamme, and G. J. Milburn. A scheme for efficient quantum computation with linear optics. *Nature*, 409(6816):46-52, 2001.

[13] J. Eisert. Optimizing linear optics quantum gates. *Phys. Rev. Lett.*, 95(4), 2005.

[14] D. L. MacFarlane, J. Tong, C. Fafadia, V. Govindan, L. R. Hunt, and I. Panahi. Extended lattice filters enabled by four-directional couplers. *Applied Optics*, 43(33): 6124-6133, 2004.

[15] N. Sultana, W. Zhou, T. LaFave Jr and D. L. MacFarlane. HBr based inductively coupled plasma etching of high aspect ratio nanoscale trenches in InP: Considerations for photonic applications. *J. Vac. Sci. B*, 27(6): 2351-2356, 2009.

[16] D. L. MacFarlane, M. P. Christensen, K. Liu, T. P. LaFave Jr., G. A. Evans, N. Sultana, T. W. Kim, J. Kim, J. B. Kirk, N. Huntoon, A. J. Stark, M. Dabkowski, L. R. Hunt, and V. Ramakrishna. Four-port nanophotonic frustrated total-internal reflection coupler. *IEEE Phot. Tech. Lett.*, 24(1):58-60, 2012.

[17] D. L. MacFarlane, M. P. Christensen, A. El Nagdi, G. A. Evans, L. R. Hunt, N. Huntoon, J. Kim, T. W. Kim, J. Kirk, T. P. LaFave Jr., K. Liu, V. Ramakrishna, M. Dabkowski, and N. Sultana. Experiment and theory of an active optical filter. *IEEE J. Quant. Electron.*, 48(3): 307-317, 2012.

[18] D. S. Gale. Frustrated total internal reflection. *Am. J. Phys.*, 40(7): 1038-1039, 1972.

 Received 30 August 2018